A Matrix Transducer Design with Improved Image Quality and Acquisition Rate

Chris Daft, Dan Brueske[†], Paul Wagner and Donald Liu[†]
Siemens Medical Solutions
Mountain View, CA and [†]Issaquah, WA, USA.
daft@ieee.org

***Abstract*—Fully sampled 2D arrays present severe and conflicting requirements in element count, interconnect density, impedance, autonomous delay and amplitude control, high bandwidth at high dynamic range, and power consumption. cMUT transducer elements can have arbitrary dimensions machined directly above integrated circuits. We have designed a circuit that fits within the area of a 2D array element and achieves good signal fidelity at practical power dissipation, while limiting interconnect to 1D array complexity. It incorporates several novel techniques that simplify the process of preamplification, time-varying gain, baseband mixing, A/D conversion and beam formation. This achieves the design goals with highly parallel information retrieval. We also describe a novel transmitter that images at high volume rates with similar penetration to a traditional probe. Such performance is useful for visualizing fast-moving anatomical structures, such as heart valves, in 3D. We show how the transmitter and receiver form a bistatic probe suitable for clinical use. Experimental data are presented to evaluate the image quality obtained from the receiver circuit. We analyze its noise, distortion and time-gain control (TGC) performance. The new approach appears competitive with 1D probes in all basic imaging parameters, and permits 3D scanning. We also investigate transmitter performance. Finally, we compare two-way signal-to-noise ratio and penetration with the state of the art.**

Keywords: *medical ultrasound; 3D; silicon ultrasound, cMUT; MEMS; capacitive micromachined transducer; volume imaging.*

I. INTRODUCTION

A perennial goal in ultrasound is to create a fully sampled 2D array with individually focused and apodized elements. Since 2D array fabrication is straightforward with silicon lithography, the problem becomes one of data rate and interconnect. Too much information is created in too small an area for traditional solutions. 2D elements' high impedance precludes driving a cable. Field-of-view and spatial sampling considerations require 5000-35000 elements, which are impractical to connect to (except in transthoracic adult cardiology arrays [1]). Aperture size cannot be reduced without severe penetration and resolution loss. We have taken advantage of our low-temperature cMUT process to create devices directly above an integrated circuit, with electrical connection through the final IC passivation [2]. Meeting this constraint makes the design of the metal layers in the IC possible, since individual channel signals are only dealt with beneath the element where the signal is generated. A further advantage of this smallest possible interconnect path from the element to the preamplifier is signal integrity. A method for reading out the complete matrix data using analog multiplexing has been reported in [3]. In this paper we consider how to obtain *digital* data from a matrix cMUT transducer. This simplifies connections to the imager, but necessitates on-chip A/D conversion. Ultrasound-speed A/D converters with usable dynamic range typically consume hundreds of milliwatts per element. Since feasible power dissipation in the probe is limited to a handful of watts, a new receiver approach is needed for these channel counts. We describe a solution meeting these constraints, and also analyze a novel transmitter suitable for use with this matrix receiver.

II. RECEIVER ARCHITECTURE

In our design, the front-end and significant portions of the imager's DSP are integrated with the transducer elements. The circuitry is located under the element to ensure that low-level analog signals never travel any significant distance. The underlying ASIC performs either partial or complete beam formation. The degree of beam formation depends on the application: it is determined by the required degree of receive beam parallelism. In all cases, however, the data produced by the array is compressed enough by beam formation that it can be moved off-chip using standard flex-circuits. Figure 1 illustrates the overall block diagram.

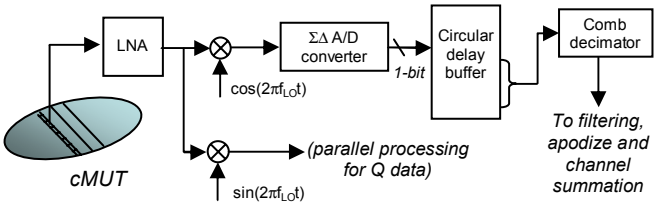

Figure 1. Front-end of monolithic probe which incorporates MEMS transduction and beam formation in the same silicon. System SNR is optimized as there is only a few µm from each element to its low-noise amplifier. Interconnect complexity characteristic of matrix probes is eased with sufficient miniaturization of the electronics. These blocks are followed by standard beamformer functions like apodize, filtering and summation.

III. RECEIVER ANALYSIS

A. Analog front-end beneath transducer element

The initial preamplifier connected to the cMUT drums is designed to balance SNR, dynamic range and power consumption. The next stage is an analog quadrature demodulator which transforms the signal to baseband. Another analog circuit implements the integrator needed in the ΣΔ loop. We characterized several designs, and obtained the noise figure and frequency response results of Figures 2 and 3 with a typical

implementation that met power, dynamic range, distortion and die area goals.

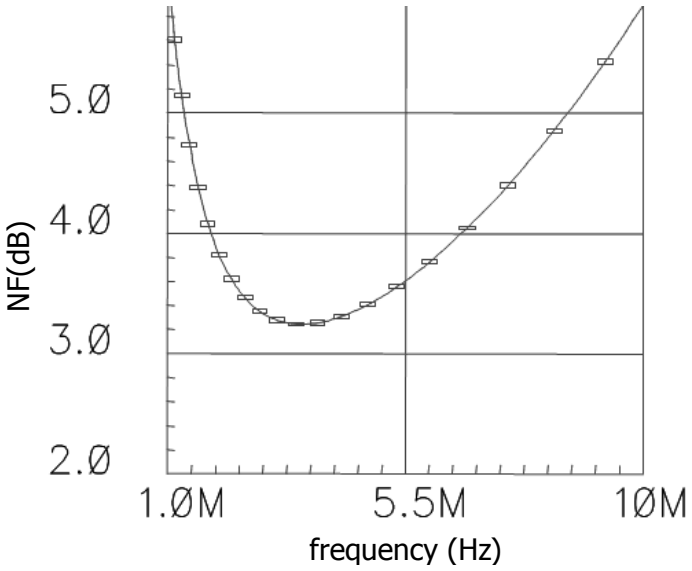

Figure 2. Noise figure of a representative front end design as a function of frequency. The line shows the extent to which the SNR is degraded from the "intrinsic" cMUT value, as defined by transduction sensitivity and noise from Brownian motion. The performance is dependent on the power dissipation.

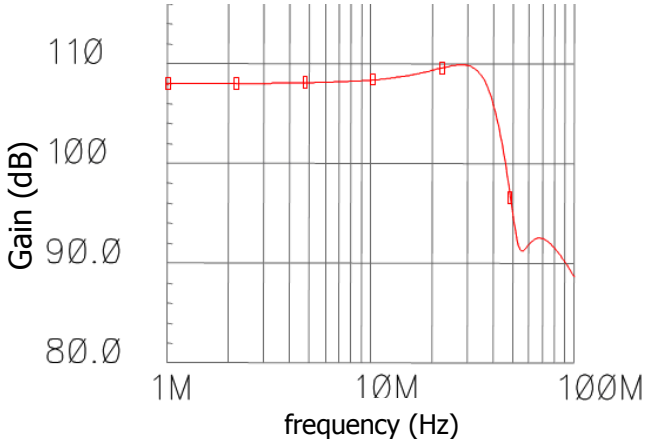

Figure 3. Frequency response of the analog electronics. The ordinate has an arbitrary reference. The circuit has ample bandwidth for imaging, and a benign phase shift variation with frequency (not shown).

B. A/D conversion beneath transducer element

A ΣΔ converter [4] uses a fast comparator that operates not on the ultrasound signal itself, but on the difference between that signal and its quantized and scaled integral (see Figure 4). This low-pass filters the signal *X*, while high-pass filtering the quantization noise *Q* (Equation 1).

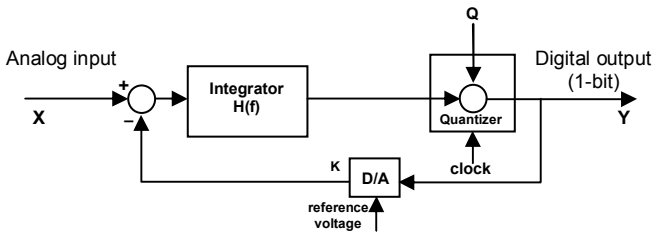

Figure 4. A ΣΔ A/D converter produces a pulse train which can be digitally low-pass filtered into a faithful representation of the analog input. The benefits of oversampling are greatly increased by shaping the noise spectrum. When the signal is converted to base-band prior to A/D conversion, we can trade off bandwidth and dynamic range to suit each imaging mode.

The **total** noise power created by the quantizer is fundamental, but its spectral distribution depends on circuit topology. In the frequency domain,

$$Y = \frac{H}{1+KH}X + \frac{1}{1+KH}Q \qquad (1)$$

The degree to which this noise shaping gains SNR via oversampling is determined by the frequency response of the integrator *H(f)*. The dynamic range *D* (in dB) is given by:

$$D = 10\log_{10}\left[1.5\left(\frac{2L+1}{\pi^{2L}}\right)\left(2^{N}-1\right)^{2}R^{2L+1}\right] \qquad (2)$$

where *L* is the order of the converter, *R* is the oversampling ratio and *N* is the number of bits in the quantizer. Figure 5 shows *D* = 70 dB achieved at 32x oversampling. The graph includes a narrow-band signal at 1% of the sampling rate. Note the high-pass filtered noise spectrum.

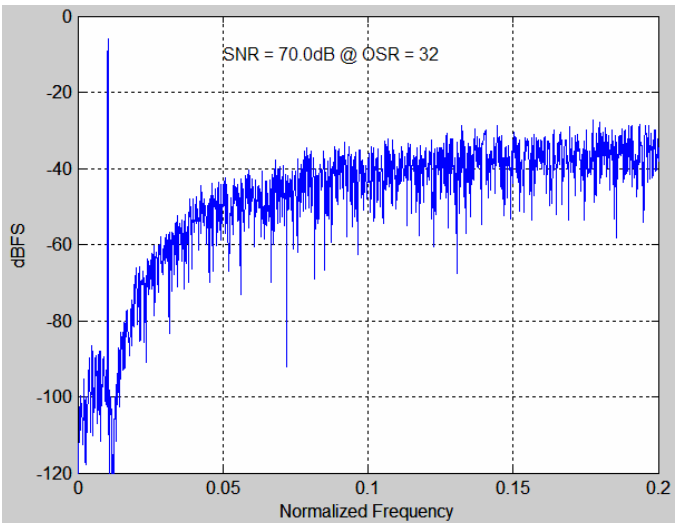

Figure 5. Spectrum of signal and noise at the output of the ΣΔ converter. Frequency is expressed as a fraction of the converter clock. Noise power is concentrated out of band by the ΣΔ modulation. Dynamic range is determined by the oversampling ratio. Unlike a traditional front-end, performance depends on the speed of the digital electronics, not analog transistor quality.

ΣΔ-based ultrasound systems were proposed at least as far back as 1992 [5]. Since then, semiconductor processes have advanced enough to allow efficient implementation of the digital filtering that replaces the troublesome analog anti-aliasing filter. Additionally, they support high clock rates for large oversampling ratios (R in Equation 2). This topology eliminates the power-hungry sample-and-hold amplifiers and wide-bandwidth gain stages essential to the pipeline ADC concept [6].

There are two further advantages specific to ultrasound. Since we are digitizing a baseband signal, R can be a function of imaging mode, so that B-mode can use high bandwidth at lower R, whereas narrow-band flow modes can increase R and thereby the dynamic range. Secondly, the beamforming delay can be efficiently accomplished while the signal is still a fast 1-bit stream, which removes the need for interpolation. This is discussed further in section IV.

C. *Time-gain control within the ΣΔ loop*

To achieve the overall dynamic range required by a modern ultrasound system (not merely a good *instantaneous* dynamic range) time-gain control (TGC) is essential. The ΣΔ loop has a feature which permits a simple implementation of this function. From Equation 1, the overall ΣΔ gain can be modulated by changing the DAC reference K that connects to the summing junction in Figure 4. Figure 6 shows the effectiveness of such an implementation, where an exponentially decreasing input signal is matched by the DAC reference so that the output amplitude does not change with depth. Echoes from the body decrease roughly exponentially with depth, but the TGC for a particular patient can be set by the user by front-panel sliders.

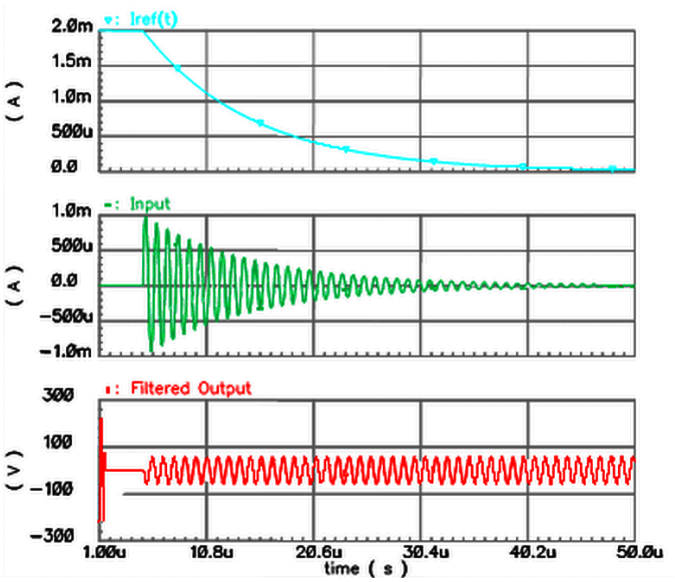

Figure 6. Time-gain control is implemented by changing the DAC's reference. Shown above are an exponentially decreasing TGC control current (blue) and a exponentially decreasing input whose amplitude is similar to tissue (green). The red line is the TGC circuit's output, showing that the decreasing amplitude has been compensated for.

Figure 7 shows the layout of the circuitry described in sections II and III.

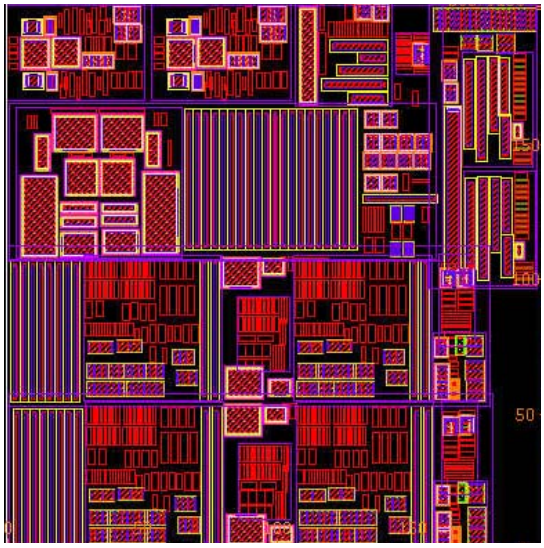

Figure 7. Layout of a complete "cell" of integrated devices positioned underneath a 2D transducer element. Metallization layers are not shown for clarity. The cell size is 200 x 200 μm.

IV. Image Quality

To gauge the image quality of this novel receiver architecture, we acquired experimental data from a 64-element transducer (1D for this evaluation) with a center frequency of 2.6 MHz and 80% half-power fractional bandwidth. Its element spacing was 0.44λ. The channel data were processed as outlined in the previous sections.

The use of ΣΔ bit-streams for beam formation is both enticing and problematic. Traditional multi-bit beamformers interpolate relatively low-speed data streams to create fractional-clock delays. The bit-serial ΣΔ data is clocked fast enough to obviate the interpolators, but it is not clear what data to insert when the beam formation demands a "clock slip", or adjustment of the time-base to compensate for changing geometric path lengths as the beam progresses.

Figure 8 compares two well-known methods for dealing with this problem with a new approach. The beamforming time stretch can be achieved by repeating the most recent sample to fill the gap in the bit-stream of +1 and –1 values. Alternatively, a value of 0 can be inserted. The effect of these schemes is shown in the first two images of Figure 8.

The third image has better quality. We achieve this by combining the decimation stage (see Figure 1) with the dynamic delay operation. This can be thought of as a non-uniform decimation. Rather than doing an M-fold decimation by summing M values from the bit-stream and then moving on to the subsequent M samples, we produce dynamic delay by sometimes adjusting the address by $(M - 1)$ samples instead of M. This implements the time-base stretch without adding fictitious samples to the incoming data. The improvement in cystic clearing is substantial.

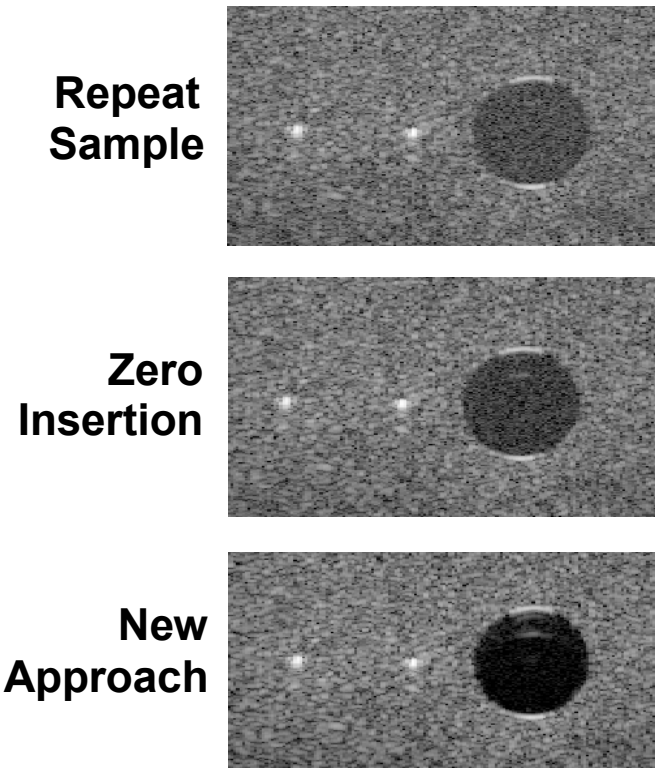

Figure 8. In each image above, the cyst diameter is 10 mm and the dynamic range shown is 60 dB. Beam formation requires dynamically changing receive delays. Implementing this for a ΣΔ 1-bit data stream has previously proved troublesome. What happens when the delay value of a given channel must slip by one convert clock? The images are of experimental data beamformed by different ΣΔ configurations. The first image was produced by repeating a sample value when the clock slips. The second inserts zero values for the missing data. A new approach is shown in the bottom image. Image quality (mostly contrast resolution) is improved with this algorithm.

Confirmation that this approach produces high beam quality can be seen in Figure 9. These receive-only beam profiles are what would be expected from this type of transducer connected to a premium-level beamformer.

V. . Transmitter Design

A. *Simple bistatic transmitter*

There are many ways to utilize a fully-sampled receive aperture. Conceptually, the simplest approach would be to integrate a transmitter under each element. In this study we chose to analyze some bistatic (separate transmit and receive aperture) approaches. These leverage the full sampling of the receive matrix to allow for simpler transmitters. An example is shown in Figure 10, where two curved, 1D arrays focus in azimuth (perpendicular to the plane of the diagram) while defocusing in elevation (the plane of the diagram).

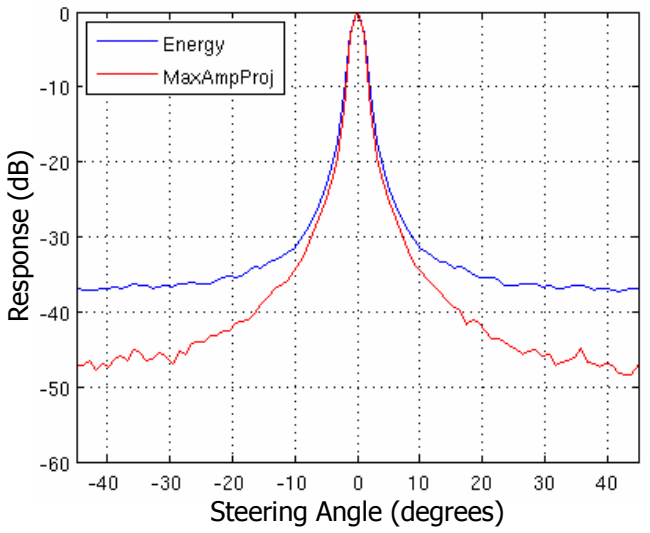

Figure 9. Two representations of the ΣΔ beamformer's point spread function. The blue beam profile shows the energy summed over range for each beam angle. The red beam profile plots the maximum response observed over range at each beam angle. These results predict good contrast and detail resolution.

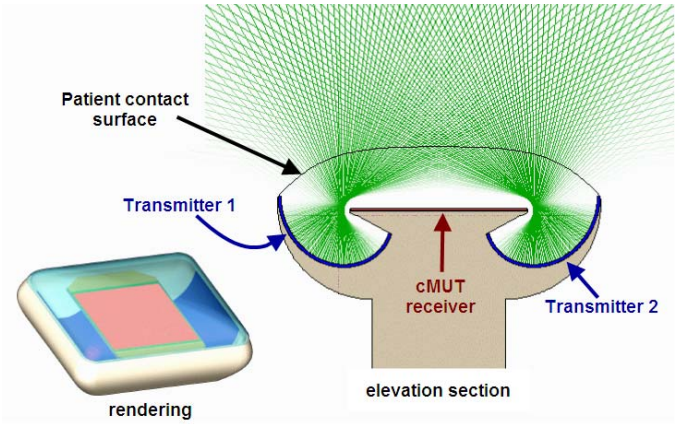

Figure 10. A bistatic probe design suitable for abdominal imaging. The receiver is as described in sections II-IV. 1D transmitters are located on two sides of the receiver matrix. The transmitters scan normally in azimuth (perpendicular to the plane of the elevation section) and form defocused beams in the plane of the diagram. A transmit aperture may be synthesized from two firings. A 3D rendering of the arrangement is shown at the left.

The novel elevation behavior is produced by focusing next to two edges of the receiver. The waves then diverge in elevation, as illustrated by the ray-tracing in Figure 10. Defocusing helps to reduce the maximum mechanical and thermal indices within the body: the peak values occur in a low-loss coupling medium. This arrangement allows for a high level of receive beam parallelism in elevation.

B. *Transmit pressure and two-way performance*

Sequential-beam transmit in azimuth, coupled with parallel transmit in elevation occupies an interesting position on the continuum balancing volume acquisition rate *vs.* per-beam power density. Point resolution equal to a transmit-receive aperture can be obtained by operating the two transmitters in a

synthetic aperture mode [7]. Synthetic aperture imaging has a number of advantages [8] over traditional approaches, such as volume acquisition rate and dynamic (retrospective) transmit focusing for fully confocal imaging.

An elevation-defocused transmitter does not produce as much acoustic *intensity* as a traditional array with a fixed elevation focus. Fewer firings are required to obtain a complete volume, since the power deposition is similar. Figure 11 illustrates the difference in transmit power density between a 1D array and an elevation-defocused design similar to that of Figure 10. We decreased the transmit center frequency from 6 MHz to 4.5 MHz to achieve rough parity in transmit intensity at depth. The two-way SNR comparison is more favorable. Without considering beam formation, the integrated receiver in this design is 6 dB more sensitive than the traditional 1D probe when normalized for area. Also, the coherence of the receive aperture is higher due to dynamic elevation beamforming. The largest transmit intensity deficit occurs in a region of the image where the SNR is high, which reduces the level of concern.

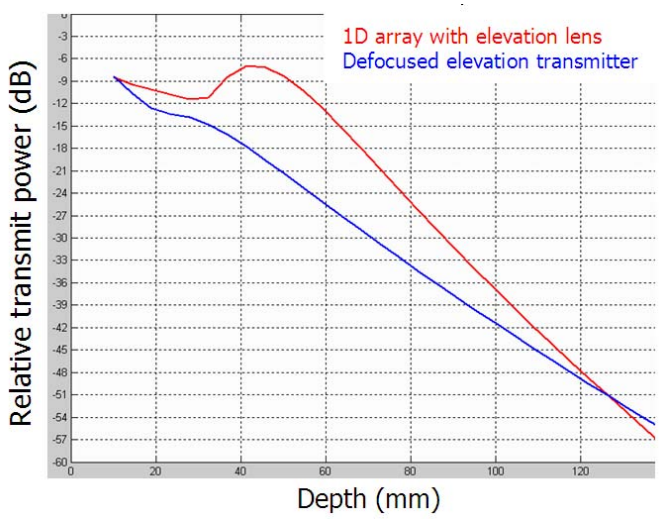

Figure 11. Transmit amplitude of an elevation-defocused transmitter, compared with a standard 1D design using an elevation lens. The apertures are the same size. Rough parity in transmit pressure at depth was obtained after the transmit frequency was reduced from 6 MHz to 4.5 MHz. Note that the matrix receiver gains 6 dB over the 1D array's receive performance.

CONCLUSIONS

Integrating a cMUT with electronics under each element offers new degrees of freedom in the design of matrix array receivers. A base-band ΣΔ A/D converter allows us to break new ground in die area and power, making possible a sub-element analog front-end and beamformer. This approach simplifies the interconnect that carries the data back to the system to a level similar to that seen in contemporary 1D probes. We have shown that the performance of a premium beamformer can be implemented under a square element with 200 µm sides.

A wide variety of transmitters can be paired with this receiver to create probes with varying complexities and costs. For example, synthetic transmit apertures can be implemented to enhance volume acquisition rate. Elevation-defocused transmitters operate at lower frequencies than traditional arrays with plastic lenses (at least until motion tracking allows more aggressive volume averaging.) The improved receive sensitivity of the cMUT design partially compensates for the transmitter power density deficit.

ACKNOWLEDGEMENTS

A number of people have contributed to this work, most prominently Kirti Patel, Brett Bymaster, Sean Hansen, Chuck Bradley, Keith Wong, Todd Willsie, Steve Martin, Brian Colby and Igal Ladabaum. We gratefully acknowledge their help.

REFERENCES

[1] Savord, B. and Solomon, R., "Fully sampled matrix transducer for real time 3D ultrasonic imaging," *Proc. 2003 IEEE Ultrasonics Symposium*, 945–953.

[2] Daft, C., Calmes, S., da Graca, D., Patel, K., Wagner, P. and Ladabaum, I., "Microfabricated ultrasonic transducers monolithically integrated with high voltage electronics," *Proc. 2004 IEEE Ultrasonics Symposium*, 493–496.

[3] Daft, C., Panda, S., Wagner, P., and Ladabaum, I., "Two Approaches to Electronically Scanned 3D Imaging Using cMUTs," *Proc. 2006 IEEE Ultrasonics Symposium,* 685-688.

[4] Candy, J.C. and Temes, G.C, "Oversampling Delta-Sigma Data Converters: Theory, Design, and Simulation," Piscataway, NJ: Wiley-IEEE Press, 1991.

[5] Noujaim, S., Garverick, S. and O'Donnell, M, "Phased array ultrasonic beam forming using oversampled A/D converters," US Patent 5,203,335.

[6] Mitteregger, G. *et al.*, "A 20-mW 640-MHz CMOS Continuous-Time ADC With 20-MHz Signal Bandwidth, 80-dB Dynamic Range and 12-bit ENOB," *IEEE J. Solid-State Circuits* **41**(12), 2641-2649 (2006).

[7] Hoctor, R.T. and Kassam, S.A. "The unifying role of the coarray in aperture synthesis for coherent and incoherent imaging," *Proc. IEEE* **78**(4), 735-752 (1990).

[8] Misaridis, T.X. and Jensen, J.A., "Space–time encoding for high frame rate ultrasound imaging," *Ultrasonics* **40**, 593–597 (2002).